WELDING RESEARCH

SUPPLEMENT TO THE WELDING JOURNAL, AUGUST, 1984

Sponsored by the American Welding Society and the Welding Research Council

Effect of Heat Treatment on the Tensile and Fracture Toughness Behavior of Alloy 718 Weldments

A modified heat treatment restores considerable fracture resistance to age-hardened weld zones without sacrificing strength

BY W. J. MILLS

ABSTRACT. The effect of heat treatment on the tensile and fracture toughness properties of alloy 718 weldments was characterized at room and elevated temperatures. The two heat treatments employed during this investigation were the conventional heat treatment (CHT), per ASTM A637, and a modified heat treatment (MHT) designed to improve the toughness of alloy 718 welds. Weldments were also examined in the as-welded condition.

CHT and MHT weldments were found to exhibit very similar tensile properties, whereas the as-welded material displayed considerably lower strengths and higher ductilities. Metallographic examination of the tensile specimens revealed that the superior ductility response in the as-welded condition was attributed to the high fracture resistance of the unaged weld matrix. The fully hardened matrix of the heat-treated weldments suppressed plastic flow in the weld zone; this resulted in higher strengths and lower ductilities.

The fracture toughness behavior of the alloy 718 welds was determined at 24, 427 and 538°C (75, 800 and 1000°F) using linear-elastic (K_{Ic}) and elastic-plastic (J_{Ic}) fracture mechanics concepts. The as-welded material exhibited the highest fracture resistance, while the CHT weld yielded very low fracture toughness values. The MHT restored considerable fracture resistance to the age-hardened weld zone without sacrificing strength. Metallographic and electron fractographic examination of alloy 718 weld fracture surfaces revealed that differences in fracture toughness behavior were associated with variations in the weld microstructures.

W. J. MILLS is with the Westinghouse Hanford Company, Richland, Washington.

Introduction

Alloy 718 is a high-strength nickel-base superalloy that possesses excellent corrosion and oxidation resistance coupled with good tensile and creep properties at elevated temperatures. In addition, alloy 718 is unique in comparison to other nickel-base superalloys, because it exhibits outstanding weldability and good resistance to strain-age cracking. The superior weldability characteristics are associated with the sluggish precipitation kinetics of the primary strengthening γ'' (body-centered-tetragonal Ni_3Nb) phase (Refs. 1,2). This sluggish age-hardening response results in a relatively low-strength, high-ductility heat-affected zone during the initial aging treatment, permitting relaxation of residual stresses and improving the strain-age cracking resistance.

Alloy 718 base metal and weldments are used in structural applications in the nuclear, aerospace and petrochemical industries where high strength, creep resistance and corrosion resistance at elevated temperatures are important design considerations. For structural components employed below 650°C (1202°F), this superalloy is generally given the conventional heat treatment (CHT), per ASTM A637—Table 1. This heat treatment, however, has contributed to a series of failures in welded components by severely reducing the impact toughness of the weld fusion zone (Refs. 3-6). The reduction in toughness has been attributed to the presence of Laves phase in the interdendritic regions of the weld metal. The CHT with a solution annealing temperature of 954°C (1750°F) does not dissolve the Laves phase in the weld zone, thereby resulting in the poor fracture resistance.

To increase the impact toughness of alloy 718 weldments, the Idaho National

Table 1—Precipitation Heat Treatments for Alloy 718

Conventional heat treatment:[a]

*Annealed at 954°C ± 8°C, air cooled to room temperature.
*Aged 8 h at 718°C ± 8°C, furnace cooled to 621°C ± 8°C and held at 621°C for a total aging time of 18 h.
*Air cooled to room temperature.

Modified heat treatment (developed by Idaho National Engineering Laboratory):[a]

*Solution annealed 1 h at 1093°C ± 8°C, cooled to 718°C ± 8°C at 55°C/h ± 28°C/h.
*Aged 4 h at 718°C, cooled to 621°C ± 8°C at 55°C/h ± 28°C/h.
*Aged 16 h at 621°C, air cooled to room temperature.

(a) Fahrenheit temperature equivalents to degrees Celsius shown are as follows: ± 28°C/h—± 50°F; 55°C/h—100°F/h; 621 ± 8°C—1150 ± 15°F; 718°C—1325°F; 1093°C—2000°F.

Table 2—Chemical Compositions, Wt-%

Element	Filler metal	Base metal	Element	Filler metal	Base metal
C	0.04	0.04	Al	0.55	0.56
Mn	0.09	0.19	Ti	1.01	1.00
Fe	17.97	Bal.	Co	0.03	0.02
S	0.007	0.002	P	0.010	0.003
Cu	0.10	0.01	Mo	3.00	3.08
Ni	53.84	53.80	B	0.004	0.005
Cr	18.04	17.65	Nb	5.11	5.24
Si	0.18	0.10	Ta	0.01	0.02

Fig. 1—Alloy 718 GTA weld

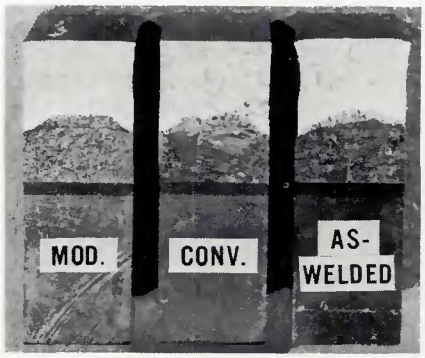

Fig. 2—Typical fracture surfaces for the MHT, CHT and as-welded alloy 718 welds

Engineering Laboratory (Refs. 6,7) developed the modified heat treatment (MHT in Table 1), which utilizes a 1093°C (2000°F) solution anneal, followed by a slow cool (55°C/hour or 100°F/h), rather than the conventional air cool. The slower cooling rates tend to reduce thermal stresses, while the higher temperature anneal dissolves the Laves phase and restores adequate impact toughness in the fusion zone (Refs. 6,7). In addition to increasing the toughness of weldments, the MHT improves the fatigue (Ref. 8) and fracture toughness (Ref. 9) responses for the base metal, while sacrificing only about 10% of the CHT material's strength (Ref. 10).

Alloy 718 weldments are usually employed in the CHT or MHT conditions for high strength applications, and in the as-welded condition for applications where high strength levels are not required. In this investigation, the tensile and fracture toughness responses of as-welded, CHT and MHT welds were characterized at room and elevated temperatures. Fracture toughness tests were performed using linear-elastic (K_{Ic}) and elastic-plastic (J_{Ic}) fracture mechanics test techniques. In addition, the fracture surface micromorphology was examined to relate key microstructural features and operative fracture mechanisms to the macroscopic properties.

Experimental Procedure

Material

Welds studied in the present investigation were produced by an automatic gas tungsten-arc (GTA) welding process, using 1.6 × 4.1 × 28 cm (0.63 × 1.6 × 11 in.) rectangular bar stock as the base metal. The compositions of the filler metal and the base metal are given in Table 2. All welds were of the single U-groove geometry as illustrated in Fig. 1. A 1.5 cm (0.59 in.) deep "J"-groove with a 0.5 cm (0.20 in.) groove radius was machined into the base metal bar stock and filled with twelve weld passes. (Specific weld procedures are outlined in Reference 10.)

Tensile Testing

Tensile tests were performed on miniature buttonhead tensile specimens with a 2.86 cm (1.125 in.) gage length and 0.32 cm (0.125 in.) gage diameter. The specimen axis was parallel to the welding direction, and the entire gage section contained only weld metal.

Tests were performed at a nominal strain rate of $3.0 \times 10^{-5}\ s^{-1}$ at temperatures ranging from 24 to 649°C (75 to 1200°F). A conventional strain-gage load cell was used to determine load, and specimen extension was based on crosshead displacement. Load and displacement values were recorded on a strip chart from which the tensile properties were determined.

Fracture Toughness Testing

Fracture toughness tests were performed on ASTM compact specimens (Ref. 11) with the notch centered in the weld deposit and oriented parallel to the welding direction. The width (W) and thickness (B) of the compact specimens were 29.3 and 12.7 mm (1.15 and 0.5 in.), respectively. All specimens were tested on an electrohydraulic closed loop machine in stroke control (stroke rate of 4.2 μm/second) at 24, 427 and 538°C (75, 800 and 1000°F). Displacements were measured on the load-line by a dual LVDT displacement monitoring technique (Ref. 12). During each test, the load-line displacement was recorded continuously on an X-Y recorder as a function of load.

Linear-elastic K_{Ic} fracture toughness tests were performed on the CHT weld at room temperature in accordance with ASTM Specification E399-81 (Ref. 11). Specimens were precracked to a crack length-to-width (a/W) ratio of 0.52 at a maximum stress intensity factor of 18 MPa$\sqrt{m}$, and subsequently loaded to fracture.

The critical load (P_Q) (obtained by the 5% secant offset procedure) and an average crack length (obtained from the surface, 1/4 thickness and 1/2 thickness positions) were used to compute the K_{Ic} fracture toughness using the standard K-solution given in ASTM Specification E399-81. The specimen size requirement to assure a valid plane strain K_{Ic} fracture toughness:

$$a,\ W\text{-}a,\ B \geq 2.5\left(\frac{K_{Ic}}{\sigma_y}\right)^2 \qquad (1)$$

where σ_y represents yield strength, was satisfied for the CHT weld at 24°C (75°F).

Nonlinear load-displacement records, which precluded the use of linear-elastic fracture mechanics techniques, were obtained for the CHT weld at elevated temperatures and the as-welded and MHT welds at all test temperatures. Under these conditions, fracture toughness tests were performed within an elastic-plastic J_{Ic} fracture mechanics framework, in accordance with the multiple-specimen J_R-curve procedures outlined in ASTM Specification E813-81 (Ref. 13).

A series of deeply cracked (fatigue precracked to a/W > 0.65 at a maximum stress intensity factor of 24 MPa$\sqrt{m}$) compact specimens were loaded to various displacements producing different amounts of crack extension, Δa, and then unloaded. After unloading, each specimen was heat tinted to discolor the crack growth region and subsequently broken open so that the amount of crack extension could be measured.

Typical fracture surfaces for the heat-treated and as-welded welds, shown in

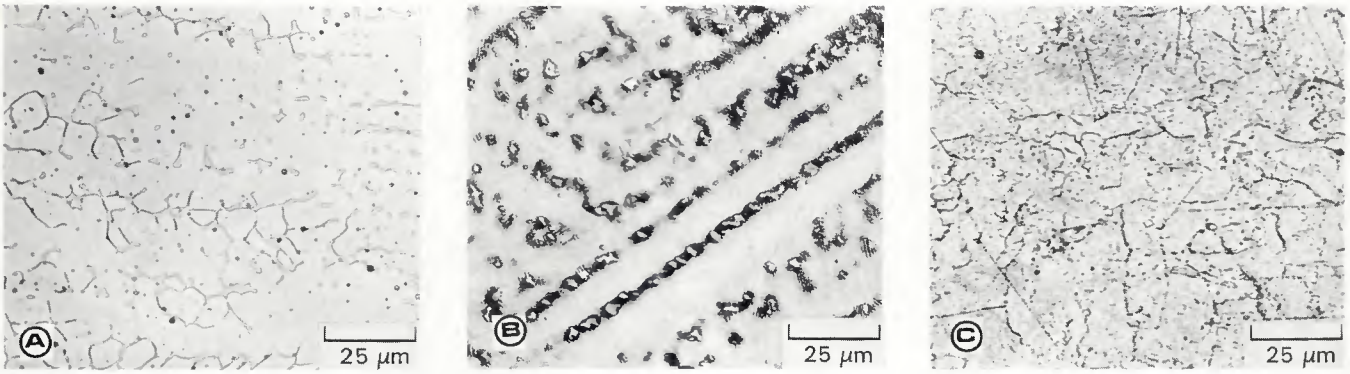

Fig. 3 — Microstructure of the weld: A — as-welded; B — CHT; C — MHT

Fig. 2, reveal that the stable crack extension region (center portion of fracture surface) was fairly uniform with maximum extension occurring in the center of the specimen. An accurate measure of Δa for each specimen was obtained by averaging crack extension values measured at nineteen positions evenly spaced across the entire crack front. The value of J was determined from the load vs. load-line displacement curve by the following equation (Ref. 13):

$$J = \frac{2A}{Bb}\frac{(1+\alpha)}{(1+\alpha^2)} \qquad (2)$$

where A = area under load vs. load-line displacement curve, b = unbroken ligament size, and $\alpha = [(2a/b)^2 + 2(2a/b) + 2]^{1/2} - (2a/b + 1)$.

The J_R-curve was constructed by plotting values of J as a function of Δa; J_{Ic} was then taken to be the value of J where a least-squares regression line through the crack extension data points intersected the stretch zone line:

$$J = 2\,\sigma_f\,(\Delta a) \qquad (3)$$

where:

σ_f = flow strength = $[\frac{1}{2}(\sigma_y + \sigma_u)]$

σ_u = ultimate strength.

The ASTM specimen size criteria for valid J_{Ic} fracture toughness determination (Ref. 13):

$$B,b > 15\frac{J}{\sigma_f} \qquad (4)$$

and:

$$B,b > 25\frac{J_{Ic}}{\sigma_f} \qquad (5)$$

were met during this investigation.

Metallographic and Fractographic Procedures

Light microscopy techniques were used to characterize the weld microstructures. Specimens were prepared by standard metallographic procedures and electrolytically etched in an oxalic acid solution to reveal the general microstructure.

Fracture surface micromorphologies were characterized by fractographic examination of test specimens on a scanning electron microscope. To relate fracture surface appearance to key microstructural features, selected areas of fracture surfaces were electropolished so that the fracture surface topography and underlying microstructure could be studied simultaneously (Ref. 14). A protective lacquer was applied to portions of the fracture surface that were to remain intact during electropolishing.

Exposed surfaces were electropolished in the following electrolyte: 25 g CrO_3, 7 ml water and 130 ml acetic acid. When electropolishing was complete, specimens were cleaned ultrasonically in acetone to remove the protective lacquer. Examination of the interfacial region between the original fracture surface and the electropolished region revealed both the fracture surface topography and underlying microstructural features.

Results and Discussion

Microstructure

The microstructure of the "as-welded" material, shown in Fig. 3A, reveals the presence of a white phase in the interdendritic regions identified by its shape and color as Laves phase. Formation of this topologically-close-packed (TCP) phase occurs during solidification in microsegregated regions enriched in Nb content. The Laves phase is believed to be responsible for the inferior impact toughness properties exhibited by alloy 718 weldments and castings (Refs. 15,16).

CHT welds exhibited a significant amount of blocky Laves phase in the interdendritic regions, as illustrated in Fig. 3B. The inability of the CHT 954°C (1750°F) postweld solution anneal to homogenize the interdendritic structure in the fusion zone was expected; in previous investigations (Refs. 3,4,6,7), temperatures in excess of 1038°C (1900°F) were required to dissolve the Laves phase. The dark regions surrounding the Nb-rich Laves phase consisted of needle-like δ precipitates, an ordered orthorhombic Ni_3Nb phase, which formed during the 954°C (1750°F) solution anneal.

The nucleation of δ needles from Laves particles is also consistent with previous observations in alloy 718 castings, whereby the Nb-rich TCP phase acted as a source for δ precipitation (Refs. 15-17). Unfortunately, the Laves phase and δ precipitates contribute little to the strength of alloy 718 weldments; moreover, they tend to act as localized crack initiation sites (as shown in the subsequent discussion).

The MHT with a 1093°C (2000°F) solution anneal drastically reduced the amount of Laves phase in the weld microstructure (Fig. 3C); this was consistent with observations made at the Idaho National Engineering Laboratory (Refs. 6,7). The higher temperature anneal apparently resulted in partial dissolution of the Laves phase, since only traces remained within the weld zone following the modified treatment.

Tensile Properties

Tensile properties for as-welded and heat-treated welds are summarized in Figs. 4 through 6; the average tensile properties for three heats of alloy 718 base metal in both the CHT and MHT conditions are also represented (see broken lines) for comparison purposes. In general, tensile properties reported herein were in agreement with those reported previously for alloy 718 welds (Refs. 7,18-21). The overall trends in tensile behavior are discussed below.

The 0.2% offset yield strength values for the CHT and MHT welds (Fig. 4) are relatively insensitive to heat treatment and temperature; they decrease from approximately 1050 MPa (152 ksi) at room temperature to 930 MPa (135 ksi) at 649°C (1200°F). Yield strength levels for the age-hardened welds were found to be equal to or greater than the aver-

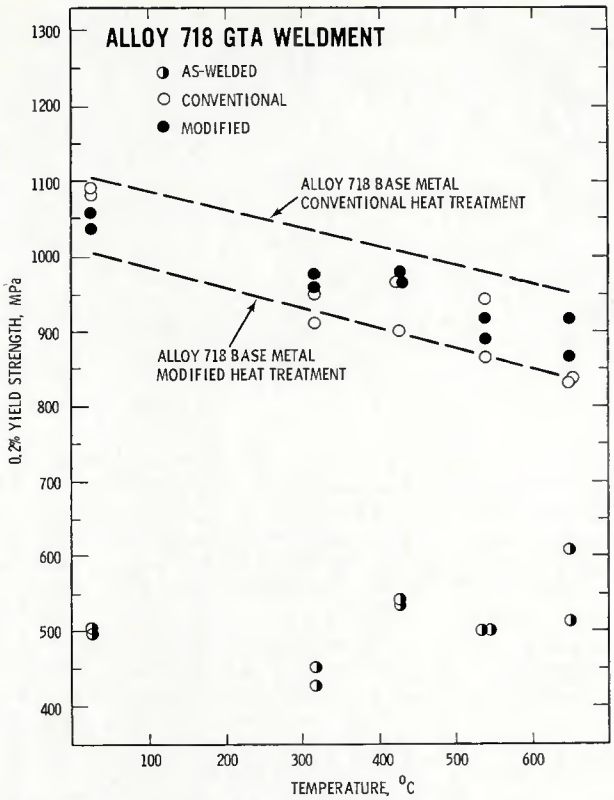

Fig. 4—Effect of temperature on the yield strength

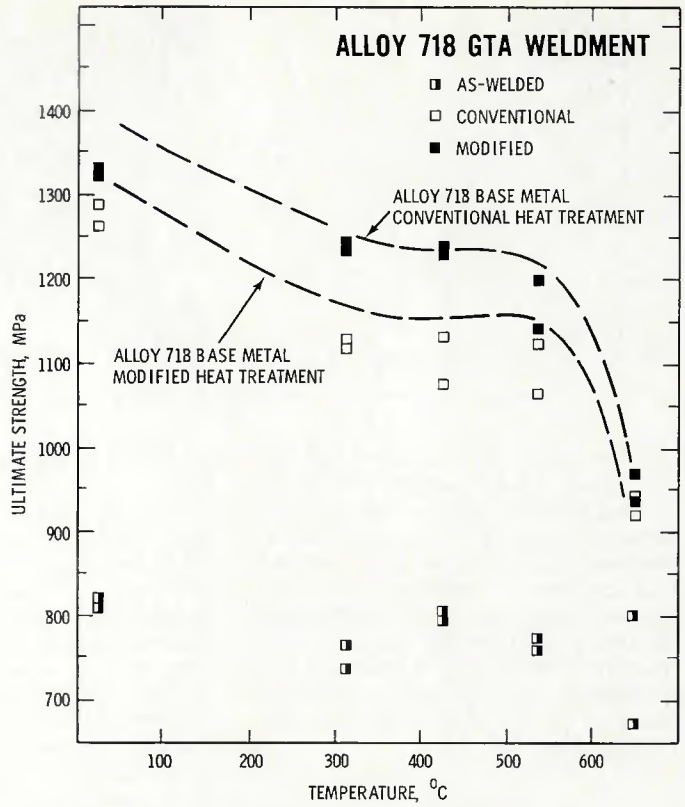

Fig. 5—Effect of temperature on the ultimate strength

age yield strength for the MHT base metal, but somewhat lower than that for the CHT base metal. As expected, the strength of the as-welded GTA weld was approximately half that for the aged material. In contrast to the tensile response of the heat-treated welds, however, the yield strength of the as-welded material increased slightly at the higher temperatures after reaching a minimum at 316°C (600°F).

Ultimate strength levels for the age-hardened welds are illustrated in Fig. 5. These were found to be in relatively good agreement with those for the base metal. The ultimate strength of the welds, like that of the base metal, was found to decrease markedly at elevated temperature. Contrasting the base metal tensile response, however, the ultimate strength for the CHT weld was generally lower than that for the MHT weld. The as-welded ultimate strength was insensitive to temperature, and was considerably lower than that for the aged material.

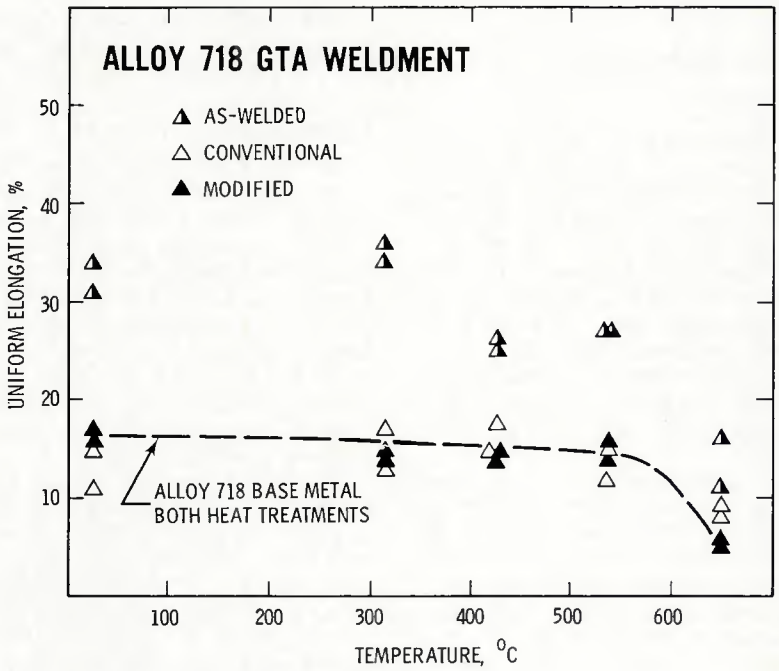

Fig. 6—Effect of temperature on the uniform elongation

Figure 6 reveals that uniform elongation values for the heat-treated welds and base metal were very similar. (Total elongation values (Ref. 10) were only 1 to 3 percentage points higher than uniform elongation values reported in Fig. 6 for both the as-welded and heat-treated conditions.) The ductility for the as-welded material is seen to be considerably greater than that for the heat-treated superalloy at temperatures up to 538°C (1000°F). At 649°C (1200°F), however, ductility values for the as-welded material rapidly approached the CHT and MHT values, suggesting that considerable age hardening occurred prior to and during the 649°C (1200°F) tensile test. To verify this hypothesis, the hardness of as-welded GTA welds aged at 316, 427, 538 and 649°C (600, 800, 1000 and 1200°F) for various periods of time were determined.

Table 3 reveals that essentially no precipitation hardening resulted from thermal aging at temperatures of 538°C (1000°F) and lower. However, the hardness of the as-welded material aged at

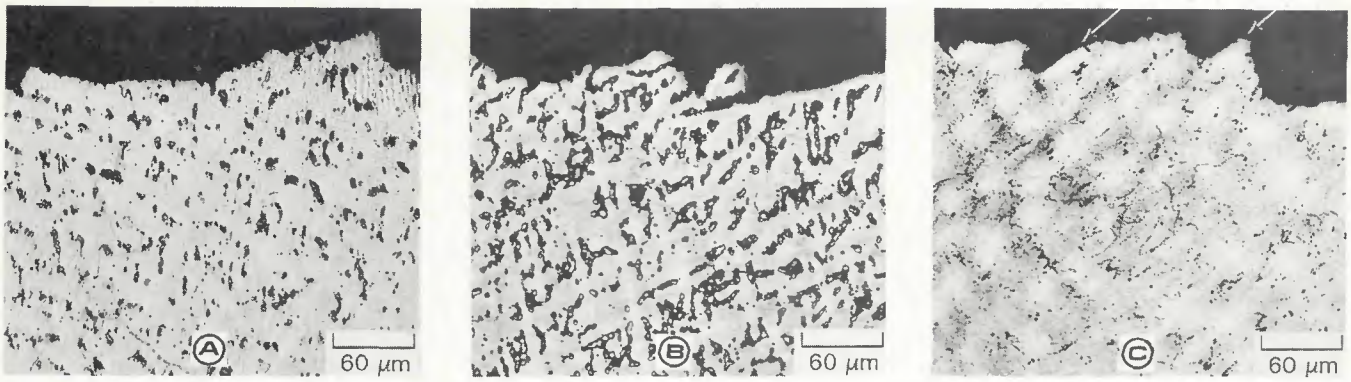

Fig. 7 — Typical metallographic fracture profiles of weld tensile specimens: A — as-welded; B — CHT; C — MHT

649°C (1200°F) rapidly approached the CHT and MHT hardness levels (R_c 41 and 40, respectively). This indicates that the drop in the as-welded tensile ductility at 649°C (1200°F) did, in fact, result from precipitation hardening during the tensile test. Furthermore, the increase in strength that resulted from the age hardening apparently offset the reduction in strength normally observed at the higher temperatures; this accounts for the strength of the as-welded alloy 718 remaining relatively insensitive to temperature over the entire test temperature range.

To characterize the effect of Laves phase on the tensile response of alloy 718 welds, metallographic fracture profiles were examined (see Fig. 7). In the as-welded material (Fig. 7A), the Laves phase fractured throughout the gage length; however, the resulting small cracks were arrested in the surrounding metal due to the high fracture resistance of the unaged nickel matrix. Hence, the ductile matrix of the unaged weld accommodates cracking of the Laves phase, which accounts for the high ductility levels. At 649°C (1200°F), the decrease in ductility was caused by a reduction in the fracture resistance of the matrix due to the substantial precipitation strengthening.

In contrast to the as-welded behavior, failure of the "brittle" Laves phase in the CHT weld was confined to the primary fracture region, as shown in Fig. 7B. Because the fracture resistance of the matrix was relatively low, due to precipitation strengthening, cracks that initiated in both the Laves and δ phases immediately grew into the low fracture resistant matrix. This explains the absence of fractured Laves particles outside the primary fracture region and the low ductility levels observed in the CHT weldment.

The MHT solution anneal significantly reduced the amount and size of the Laves phase present in the weld fusion zone. However, remnants of the original interdentritic structure were still present, as indicated by the series of dark and light regions in Fig 7C. Note that in some regions (indicated by arrows) the crack propagated along this prior interdendritic structure; this was because the remaining small Laves particles still acted as microvoid nucleation sites and thereby provided a preferential crack path.

Table 3—Effect of Aging on the Room Temperature Hardness of As-Welded Alloy 718 GTA Weldments, Rockwell C[(a)]

Aging temperature, °C	Aging time, hours					
	0	1	3	10	30	100
316	24	–	24	23	24	–
427	24	–	25	22	24	–
538	24	–	24	26	28	28
649	24	30	35	37	40	42

(a) Hardness of CHT weldment — R_c 41; hardness of MHT weldment — R_c 40.

Fracture Toughness Behavior

The CHT weld exhibited a brittle response at 24°C (75°F) as indicated by the load vs. displacement curve shown in Fig. 8. Values of K_{Ic} ranged from 62 to 73 MPa$\sqrt{m}$ — Table 4. These values were slightly higher than the fracture toughness (55 MPa$\sqrt{m}$) determined by Pettit, *et al.* (Ref. 22) and Lorenz (Ref. 24) during fracture testing of alloy 718 GTA weld specimens containing surface flaws.

The room temperature J_{Ic} fracture toughness responses for as-welded and MHT welds are summarized in Fig. 9 and Table 4. The as-welded material exhibited the higher fracture toughness, 160 kJ/m^2 (914 in.-lb/in.^{2}), while the J_{Ic} value for the MHT weld was 140 kJ/m^2 (799 in.-lb/in.^{2}). Equivalent plane strain fracture toughness (K_{Jc}) values were computed from these experimental J_{Ic} values by the following equation (Ref. 25):

$$K_{Jc} = \sqrt{\frac{J_{Ic}\,E}{(1-\nu^2)}} \qquad (6)$$

where E = Young's modulus and ν = Poisson's ratio.

The room temperature K_{Jc} values for as-welded and MHT welds (187 and 176 MPa$\sqrt{m}$, respectively — see Table 4) were much higher than the K_{Ic} fracture toughness exhibited by the CHT weld.

At room temperature, the CHT weld failed in an unstable mode, whereas the as-welded and MHT welds exhibited stable tearing at J levels well above J_{Ic}. To characterize the material's resistance to tearing, the tearing modulus (T) was determined using the following equation (Ref. 26):

$$T = \frac{dJ}{da}\frac{E}{\sigma_f^2} \qquad (7)$$

The value of T depends on the slope of the J_R curve (dJ/da) as well as the material's flow strength and Young's modulus (E). The as-welded material exhibited a very high tearing modulus (T = 101 — see Table 4) as a result of its steep slope (dJ/da = 221 MPa$\sqrt{m}$) coupled with a relatively low flow strength (σ_f = 660 MPa$\sqrt{m}$). The value of T for the MHT weld (T = 9) was an order of magnitude lower than that of the as-welded material, while the CHT weldment possessed essentially no resistance to tearing (T $\approx$ O).

The elevated temperature J_{Ic} fracture toughness responses are given in Table 4 and Figs. 10 and 11. At both 427 and 538°C (800 and 1000°F), the as-welded material yielded the highest J_{Ic} values, *i.e.*, 183 and 228 kJ/m^2 (1045 and 1302 in.-lb/in.^{2}), respectively. The CHT consistently resulted in the lowest fracture toughness (32 kJ/m^2 or 183 in.-lb/in.^{2} at both elevated test temperatures), while MHT yielded intermediate J_{Ic} values of 117 kJ/m^2 at 427°C (668 in.-lb/in.^{2} at 800°F) and 100 kJ/m^2 at 538°C (571

Table 4—Summary of Fracture Toughness Response of Alloy 718 GTA Weldments

Condition	Temperature, °C	(°F)	J_{Ic}, kJ/m²	K_{Ic} or K_{Jc}, MPa $\sqrt{m}$	$\frac{dJ}{da}$, MPa	$T\left(=\frac{dJ}{da}\frac{E}{\sigma_f^2}\right)$
Conventional	24	(75)	21[a]	62, 67, 70, 73 } 68	–	–
Modified	24	(75)	141	176[a]	62	9
As-welded	24	(75)	160	187[a]	221	101
Conventional	427	(800)	32	78[a]	21	4
Modified	427	(800)	117	150[a]	69	10
As-welded	427	(800)	183	187[a]	283	112
Conventional	538	(1000)	32	76[a]	28	4
Modified	538	(1000)	100	136[a]	82	13
As-welded	538	(1000)	228	205[a]	221	94

(a) Calculated based on equation (5): $K_{Jc} = \sqrt{\frac{J_{Ic}E}{(1-\nu^2)}}$.

in.-lb/in.² at 1000°F). Equivalent K_{Jc} fracture toughness levels are reported in Table 4.

In addition to exhibiting the highest fracture toughness values, the as-welded material also possessed superior tearing resistance under elevated temperature conditions as evidenced by its steep J_R curves. At 427 and 538°C (800 and 1000°F), values of T for the as-welded GTA weld (112 and 94, respectively) were an order of magnitude greater than tearing moduli for MHT welds (Refs. 10,13). The CHT resulted in the lowest tearing modulus (T = 4).

The room and elevated temperature J_{Ic} fracture toughness responses for base metal (Ref. 9) and welds (represented by solid and broken lines, respectively) are summarized in Fig. 12. The inferior fracture resistance of the CHT base metal relative to the MHT material was attributed to the presence of coarse δ precipitates which initiated premature microvoid coalescence (Ref. 9). The higher solution annealing temperature employed during the MHT dissolved the δ phase, resulting in higher J_{Ic} values. The MHT weld exhibited J_{Ic} values 15 to 25% lower than its base metal counterpart, but 65 to 80% higher than the CHT base metal.

Fracture toughness values for the CHT weld were much lower than base metal J_{Ic} levels. Therefore, weldments should be used in the MHT condition for high strength applications where fracture toughness is a primary design consideration. The as-welded material exhibited

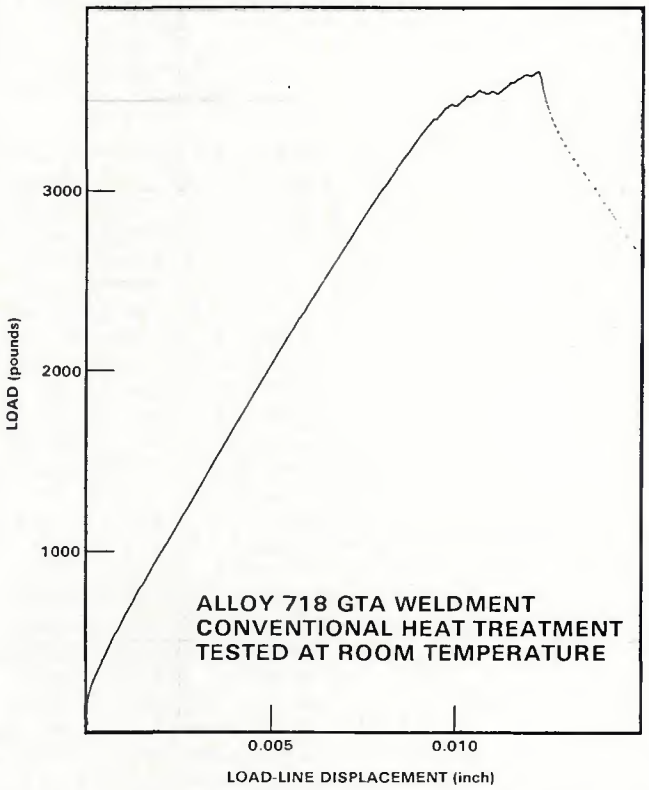

Fig. 8—Load vs. load-line displacement curve for a CHT weld at room temperature (1 lbf = 4.448 N; 1 in. = 25.4 mm)

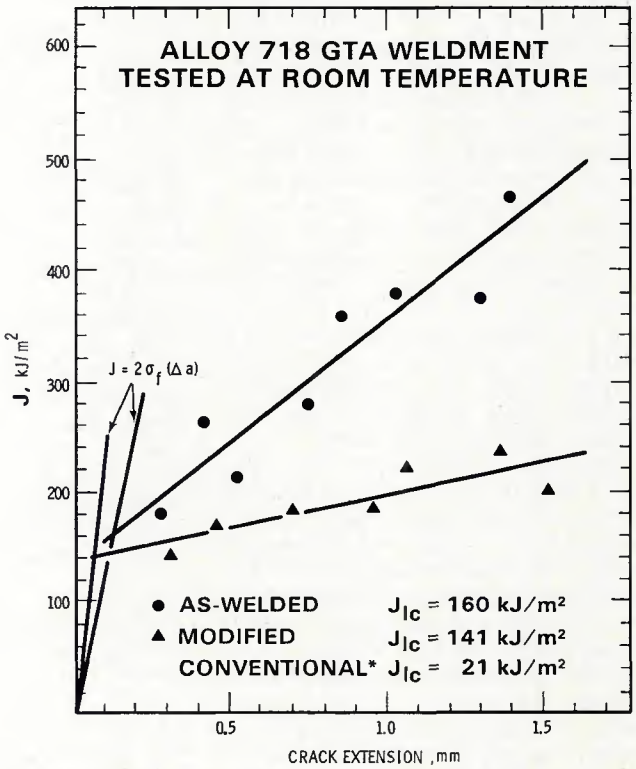

Fig. 9—J_R curves for welds tested at room temperature. The J_{Ic} value for the CHT weld was calculated from an average K_{Ic} value based on equation (6)

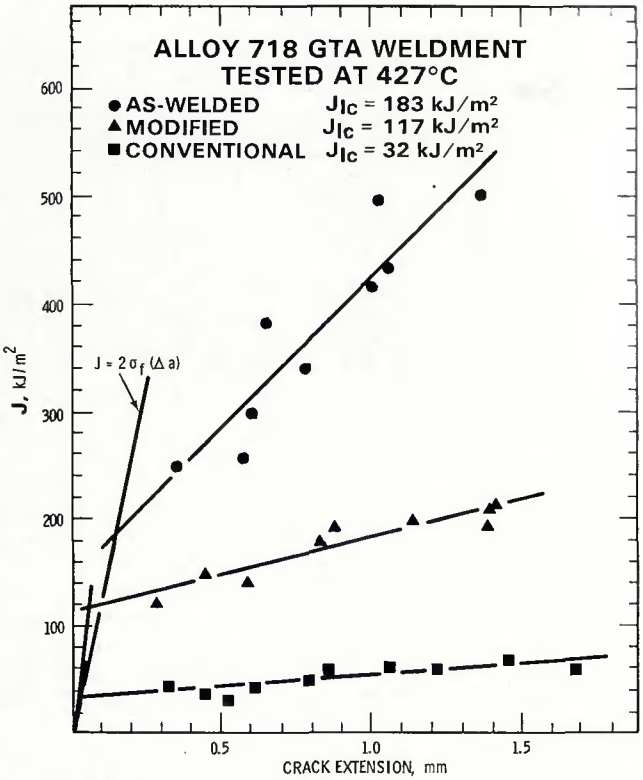

Fig. 10 — J_R curves for welds tested at 427°C (800°F)

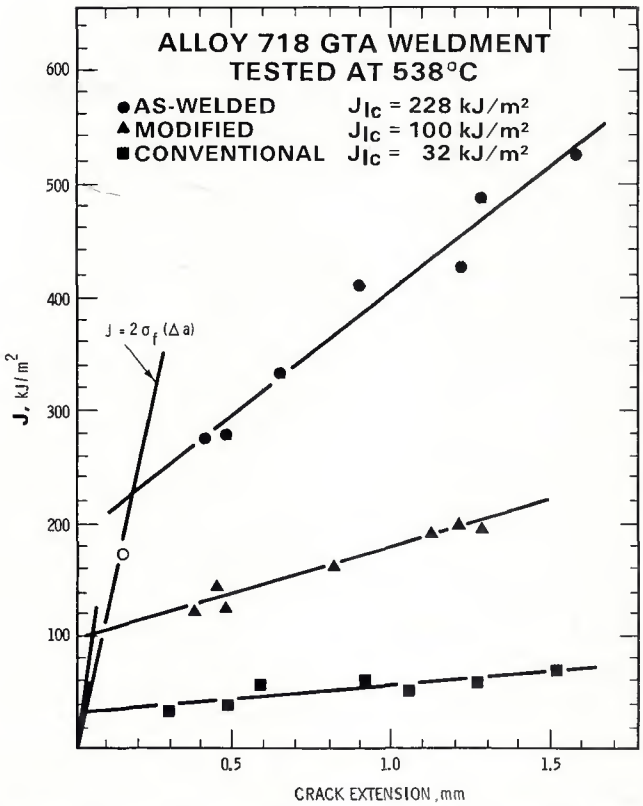

Fig. 11 — J_R curves for welds tested at 538°C (1000°F). Open data point denotes stretch zone formation

the highest fracture resistance, particularly at 427 and 538°C (800 and 1000°F). However, it sacrifices significant strength for this increased fracture toughness behavior.

Optical and electron microscopic examination of weld fracture surfaces was performed to characterize the effect of microstructure on the fracture toughness response. Metallographic fracture profiles of toughness specimens were found to be very similar to the tensile profiles shown in Fig. 7; hence, they are not reported herein. In the as-welded condition, small cracks emanating from the broken Laves particles were arrested in the ductile unaged matrix; this accounts for the very high fracture toughness values.

Electron fractographic examination of as-welded J_{Ic} specimens revealed a dimple rupture network initiated by fractured Laves particles (Fig. 13A) at all test temperatures. The well-defined rows of dimples evident in Fig. 13 were attributed to the alignment of Laves phase in the interdendritic regions. Selected area electropolishing (Fig. 13B) demonstrated that the rows of dimples shown in the left side of the metallographic-fractographic interface were, in fact, aligned with the underlying interdendritic Laves particles.

In the CHT weldment, failure of the Laves phase was confined solely to the region immediately adjacent to the fracture surface. The low fracture-resistant matrix of the age-hardened weld could not arrest cracks initiated by the Laves phase. Consequently, these localized cracks coalesced into the primary crack front before other particles further removed from the crack could fail.

The CHT weld fracture surfaces also exhibited rows of dimples (Fig. 14A) that nucleated at the interdendritic Laves and

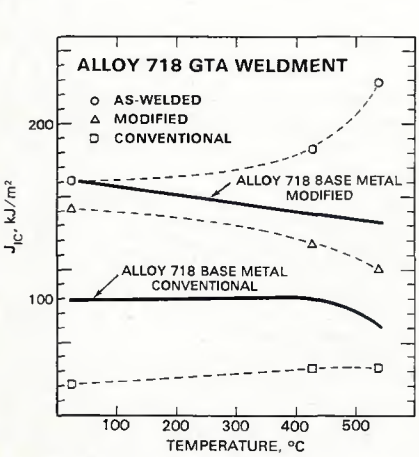

Fig. 12 — Effect of temperature on fracture toughness response

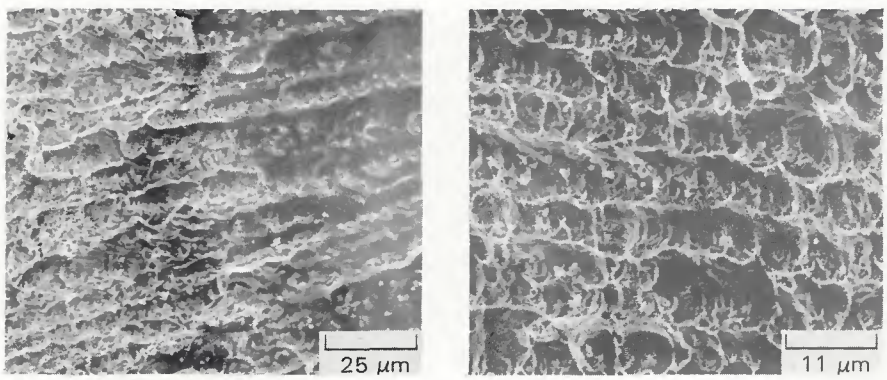

Fig. 13 — Electron fractographs of the as-welded fracture surfaces: A — rows of dimples; B — metallographic-fractographic interface

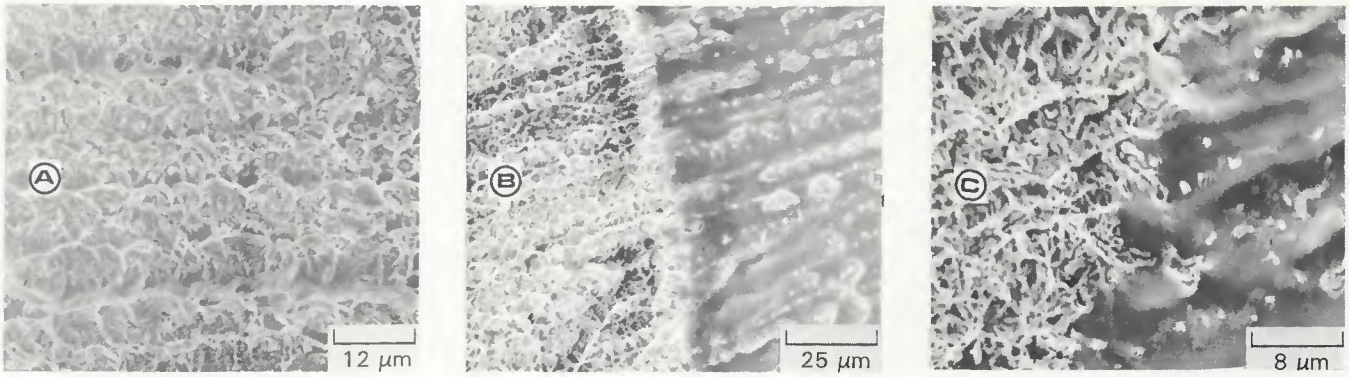

Fig. 14 — Electron fractographs of CHT fracture surfaces: A — rows of dimples; B — metallographic-fractographic interface; C — higher magnification of metallographic-fractographic interface revealing Laves and δ particles

δ particles, as shown in Figs. 14B and 14C. Compared to the well-defined dimple rupture network observed in the as-welded condition, dimples displayed by the CHT material were rather shallow and poorly defined. The ill-defined dimples resulted from a combination of the high density of microvoid nucleation sites and the high strength matrix that suppressed plastic flow around the interdendritic particles. Moreover, the presence of coarse Laves and δ particles in the weld zone coupled with the low fracture-resistant matrix resulted in the very low fracture toughness values exhibited by the CHT weldment.

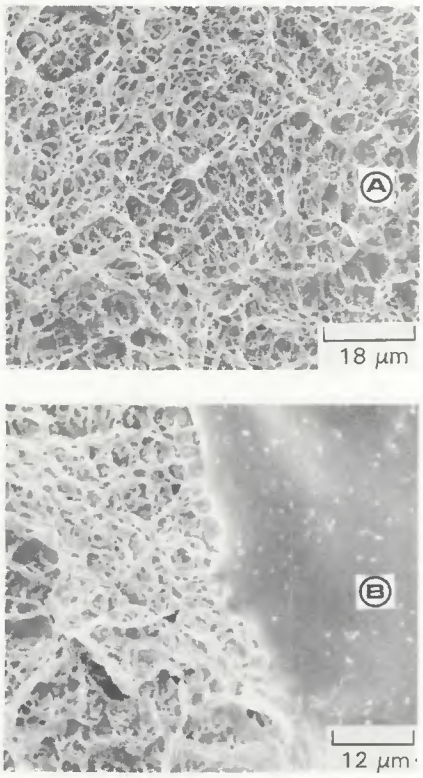

Fig. 15 — Electron fractographs of MHT fracture surfaces: A — equiaxed microvoid coalescence; B — metallographic-fractographic interface

Fracture surfaces for the MHT weld exhibited nonaligned dimples (Fig. 15A) that were initiated by Laves phase remnants in the fusion zone — Fig. 15B. The MHT homogenized the microstructure by dissolving most of the coarse second phase particles from the interdendritic regions, leaving only traces of Laves phase distributed uniformly throughout the matrix. Microvoids in the MHT weld nucleated by decohesion of the Laves particle-matrix interface, rather than by catastrophic failure of the Laves phase as observed in the as-welded and CHT conditions. Hence, the small Laves particles remaining after the MHT were apparently more resistant to fracture than the coarse particles in the other two conditions. By drastically reducing both the size and number of coarse second phase particles in the weld zone, the MHT significantly improved the fracture toughness response of the age-hardened weld.

Conclusion

The tensile and fracture toughness behavior of as-welded, CHT and MHT alloy 718 welds was characterized at room and elevated temperatures. The results of the current investigation may be summarized as follows:

1. The strength and ductility responses for precipitation-strengthened welds were relatively insensitive to heat treatment and were comparable to base metal strength and ductility values. Contrary to fracture toughness behavior, dissolution of Laves and δ phases from the weld zone during the MHT had little effect on the weld's tensile behavior.

2. In the as-welded condition, welds exhibited lower strength levels and higher ductilities relative to those observed in the heat-treated welds. The fracture-resistant matrix in the unaged weld arrested microcracks initiated by broken Laves particles, thereby resulting in high ductility levels.

3. The as-welded material exhibited the highest fracture toughness, while the CHT weld yielded the lowest toughness values. The MHT resulted in intermediate fracture toughness levels that were comparable to base metal J_{Ic} values.

4. In the as-welded condition, small cracks emanating from fractured Laves particles were arrested by the surrounding ductile matrix. This behavior resulted in the superior fracture resistance exhibited by the as-welded material.

5. The inferior fracture toughness for the CHT weld was attributed to the low fracture resistance of the aged weld matrix coupled with the presence of many coarse Laves and δ particles that served as microvoid nucleation sites.

6. The high temperature MHT anneal significantly reduced the size and density of coarse second phase particles from the weld zone which enhanced fracture resistance without sacrificing strength.

Acknowledgment

This paper is based on work performed under U. S. Department of Energy (DOE) contract DE-AC14-76FF02170 with the Westinghouse Hanford Company, a subsidiary of Westinghouse Electric Corporation. The author wishes to express his appreciation to W. D. Themar who was most helpful in conducting these tests.

References

1. Prager, M., and Shira, C. S. 1968. *Welding of Precipitation-Hardening Nickel-Base Alloys.* Welding Research Council bulletin no. 128.

2. Duvall, D. S., and Owczarski, W. A. 1969. Studies of postweld heat-treatment cracking in nickel-base alloys. *Welding Journal* 48(1):10-s to 22-s.

3. Gordine, J. 1971. Some problems in welding Inconel 718. *Welding Journal* 50(11):480-s to 484-s.

4. Graber, M. J., Brinkman, C. R., and Hobbins, R. R. 1975. *Metallurgical evaluation of welding and heat treating procedures for the Inconel 718 PBF in-pile tube.* Report ANCR-1087. Idaho Falls: Aerojet Nuclear Company.

5. Smolik, G. R. 1974. *Analyses of failure which occurred during heat treatments of the*

Inconel 718 PBF acoustic filter. Report ANCR-1178. Idaho Falls: Aerojet Nuclear Company.

6. Smolik, G. R., and Reuter, W. G. 1975. *Heat treatment investigations for welded Inconel 718 pressure vessels for the power burst facility."* Report ANCR-1227. Idaho Falls: Aerojet Nuclear Company.

7. Reuter, W. G. 1977. *Design data for the 1/4 in. thick alloy 718 in-pile tube.* Report TREE-NUREG-1087. Idaho Falls: EG&G Idaho, Inc.

8. Mills, W. J., and James, L. A. 1978. *Effect of heat-treatment on elevated temperature fatigue-crack growth behavior of two heats of alloy 718.* ASME publication 78-WA/PVP-3.

9. Mills, W. J. 1980. The effect of heat treatment on the room temperature and elevated temperature fracture toughness response of alloy 718. *Journal of Engineering Materials and Technology* 102:118-126.

10. Mills, W. J. 1979. *The influence of heat-treatment on the microstructure and mechanical properties of alloy 718 base metal and weldments.* Report HEDL-TME 78-54, Westinghouse Hanford Company.

11. American Society for Testing Materials. 1982. .Plane strain fracture toughness of metallic materials. *1982 annual book of ASTM standards,* part 10, pp. 592-622. ASTM specification E399-81. Philadelphia, Pennsylvania.

12. Mills, W. J., James, L. A., and Williams, J. A. 1977. A technique for measuring load-line displacements of compact ductile fracture toughness specimens at elevated temperatures. *Journal of Testing and Evaluation* 5(6):446-451.

13. American Society for Testing Materials. *1982 annual book of ASTM standards,* part 10, pp. 822-840. ASTM specification E813-81. Philadelphia, Pennsylvania.

14. Chesnutt, J. C., and Spurling, R. A. 1977. Fracture topography microstructure correlations in the SEM. *Metallurgical Transactions* 8A:216-218.

15. Eiselstein, H. L. 1963. Metallurgy of columbium-hardened nickel-chromium-iron alloy. *Advances in the Technology of Stainless Steel and Related Alloys,* ASTM STP no. 369, pp. 62-77.

16. DeVries, R. P., and Mumau, G. R. Importance of a Relationship Between Dendrite Formation and Solidification in Highly Alloyed Materials. *Journal of Metals* 20(11):33-36.

17. Barker, J. F. 1962. A superalloy for medium temperatures. *Metal Progress* 81:72-76.

18. Korth, G. E., and Smolik, G. R. 1978. *Status report of physical and mechanical test data of alloy 718.* Report TREE-1254. Idaho Falls: EG&G Idaho, Inc.

19. Ward, A. L., Steichen, J. M., and Knecht, R. L. 1976. Irradiation and thermal effects on the tensile properties of Inconel 718. *Irradiation effects on the microstructure and properties of metals,* pp. 156-170. ASTM STP 611. Philadelphia, Pennsylvania: American Society for Testing Materials.

20. Huntington Alloy Products Division, The International Nickel Company, Inc. 1973. INCONEL alloy 718. Huntington, West Virginia.

21. Mayor, R. A. 1976. Selected mechanical properties of Inconel 718 and 706 weldments. *Welding Journal* 55(9):269-s to 275-s.

22. Pettit, D. E., Fedderson, C. E., and Mindlin, H. 1969. *Flaw growth behavior of Inconel 718 at room and cryogenic temperatures.* NASA report CR-101942. Columbus, Ohio: Battelle-Columbus Laboratories.

23. Forman, R. G. 1974. *Crack-growth behavior in thick welded plates of Inconel 718 at room and cryogenic temperatures.* NASA report TN D-7665. Houston, Texas: Lyndon B. Johnson Space Center.

24. Lorenz, P. M. *Effect of pressurized hydrogen upon Inconel 718 and 2219 aluminum.* Report prepared for Jet Propulsion Laboratory EG-479375 and University of California at Berkeley G845350. Seattle, Washington: Boeing Company.

25. Begley, J. A., and Landes, J. D. 1974. The J integral as a fracture criterion. *Fracture toughness,* pp. 1-20. ASTM STP 514. Philadelphia, Pennsylvania: American Society for Testing Materials.

26. Paris, P. C., Tada, H., Zahoor, A., and Ernst, H. 1979. The theory of instability of the tearing mode for elastic-plastic crack growth. *Elastic-plastic fracture,* pp. 5-36. Philadelphia, Pennsylvania: American Society for Testing Materials.

A Reminder to Authors

If you plan to present a paper at the 66th Annual AWS Convention, April 29-May 3, 1985, be sure to get your 500-word summary with the Author Application Form (opposite page 166-s, May issue) into the mail no later than August 15, 1984. (An "Invitation to Authors" with further instructions also appeared in May—see page 84.)

For papers to be presented at the 16th AWS International Brazing and Soldering Conference, April 30-May 2, 1985, the Author Application Form (opposite the Reader Information Card, April) and abstract must be mailed no later than August 15, 1984.

WRC Bulletin 286
August, 1983

Fatigue Behavior of Aluminum Alloy Weldments

by W. W. Sanders, Jr. and R. H. Day

This report provides a summary and overview of the fatigue behavior of aluminum alloy weldments. In 1972, a first state-of-the-art report, WRC Bulletin 171, was prepared and a computerized data bank was initiated. This report has emphasized the knowledge gained since the publication of that first summary and indicates the extent of the data added to the bank.

Publication of this report was sponsored by the *Aluminum Alloys Committee* of the *Welding Research Council.* The price of WRC Bulletin 286 is $12.75 per copy, plus $5.00 for postage and handling. Orders should be sent with payment to the Welding Research Council, Room 1301, 345 E. 47th Street, New York, NY 10017.